Politecnico di Torino

Bachelor's Degree in Mechanical Engineering
Department of Energy (DENERG)

Impact of material change on thermo-structural behaviour of F-class gas turbine discs

Academic year:
2023-2024

Supervisors:
Prof. Dr. Daniela Anna Misul,
Annalisa Maragno (EthosEnergy)

Candidate:
Perfetti Massimo 298588

Contents

Table of Contents

1 Premises

This research, conducted in collaboration with EthosEnergy S.p.A., aims to perform a thermo-structural analysis focusing on the behavior of turbine discs in response to changes in their constituent materials. The specific components under analysis are the discs of a FR1500 gas turbine Figure 1, manufactured by EthosEnergy S.p.A. at their facility in Settimo Torinese (TO). The FR1500 gas turbines commenced their commercial operation in 1990 and continue to be operational and producing electricity nowadays. With over 950 installed units, these turbines collectively generate approximately 175 GW of power across 11 countries. The purpose of the thesis is to assess the advantages and disadvantages of transitioning from the NiCrFe alloy - NiCrFe alloy to the NiCoCr alloy - NiCoCr alloy for the production of turbine components.

The primary objective is to evaluate the thermal and structural impacts on the rotor throughout its operational cycle, from start-up to shutdown, utilizing transient 2D thermal-structural analyses with ANSYS Mechanical. Emphasis will be placed on examining stresses and deformations for both possible materials, comparing them against design tolerances and material limit curves to assess their acceptability. The comparative analysis of the resulting data will help determine whether one of the examined materials is more suitable than the other for the specific application or if both materials are equally viable.

1.1 EthosEnergy S.p.A.

EthosEnergy S.p.A. is a leading company that provides services and solutions for the power and oil and gas industries. The company specializes in the maintenance, repair, and overhaul of rotating equipment such as gas and steam turbines, generators, and compressors. In particular, the Settimo Torinese facility is exclusively used for the production of gas turbines.
Some processed data during the discussion, including graphs and considerations, will be redacted or normalized due to a non-disclosure agreement with respect to the corporate databases.

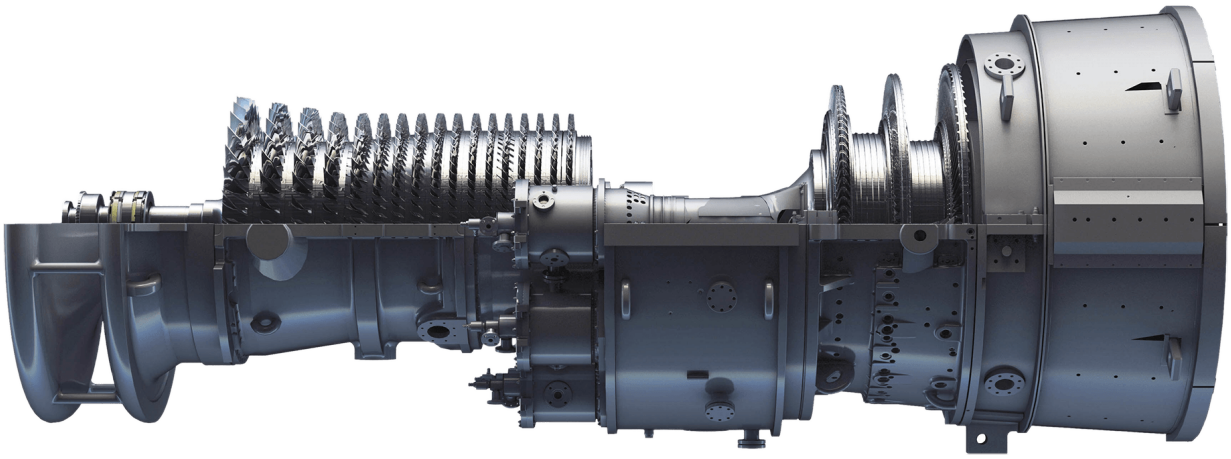

Figure 1: Section of a FR1500 gas turbine

2 Introduction

2.1 Gas turbines: overview and components

A gas turbine, commonly known as a turbogas, operates through a sequence of processes involving three primary components: the compressor, the combustor, and the turbine, as shown in Figure 2. Initially, air is drawn into the compressor (1), where it is pressurized to significantly higher levels, thereby increasing its temperature and density (2). This compressed air then enters the combustor, where it is mixed with fuel and ignited. The combustion process generates a high-temperature, high-pressure gas (3), which then flows into the turbine section. There, it expands through a series of turbine blades, imparting energy to the turbine blades and causing the turbine to spin. This mechanical energy is then harnessed both to drive the compressor and to generate power, completing the cycle. Finally, considering a simple cycle, exhaust gases leaving the turbine are not re-circulated and therefore they are expelled into the environment (4).

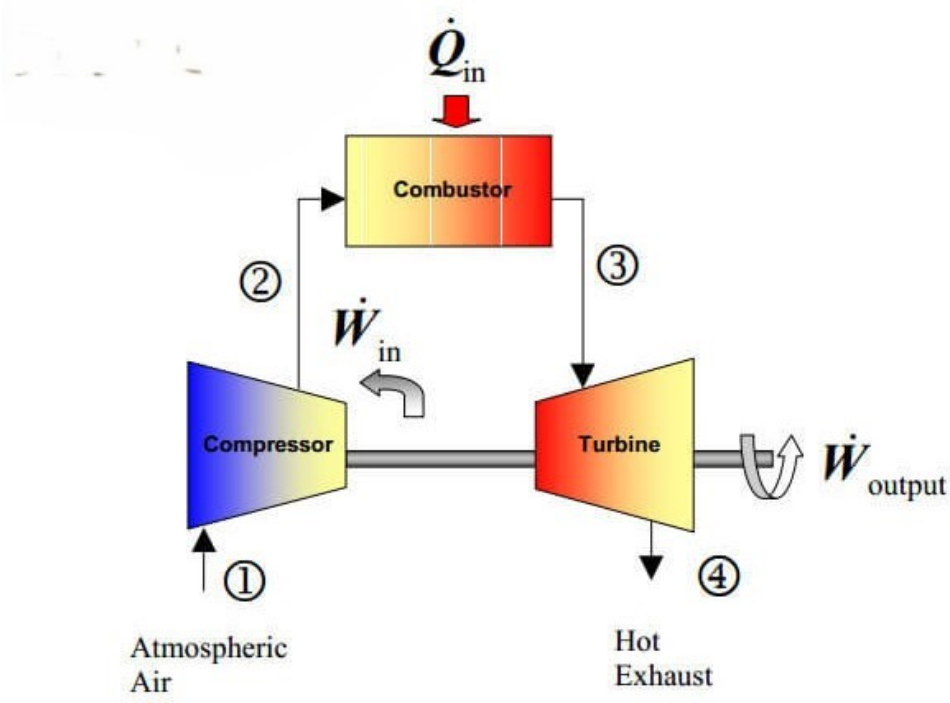

Figure 2: System representation of Gas Turbine simple cycle

During the initial process required to set the gas turbine in motion, an external work input provided by outside is necessary to spin the compressor. The compressor, once in motion, generates negative work due to the energy it consumes to compress the air. Conversely, the turbine itself produces positive work by converting the energy from gases into mechanical energy. For the gas turbine to function effectively and produce a net positive work output, the positive work generated by the turbine must exceed the negative work required by the compressor. One last important feature is that the turbine and the compressor are mechanically connected via a common shaft, which is also known as the rotor. This interconnected system ensures that the energy conversion process is continuous and efficient.
The net work output (W_{net}) of a gas turbine plant is calculated as the difference between the work produced by the turbine (W_T and the work consumed by the compressor (W_C. The mathematical expression for the net work output is:

$$W_{\text{net}} = W_T - W_C = \dot{m} \cdot [(h_3 - h_4) - (h_2 - h_1)]$$

With:

- $\dot{m}$ being the mass flow rate of the working fluid (air and combustion gases).
- h_3 and h_4 representing the specific enthalpies at the turbine inlet and outlet, respectively.
- h_1 and h_2 being the specific enthalpies at the compressor inlet and outlet, respectively.

Moreover, the thermal efficiency (η_{th}) of the gas turbine plant can be calculated as the ratio of the net work output to the heat added in the combustor (Q_{in}):

$$\eta_{\text{th}} = \frac{W_{\text{net}}}{Q_{\text{in}}} = \frac{(h_3 - h_4) - (h_2 - h_1)}{h_3 - h_2}$$

Where the heat added in the combustor (Q_{in}) is given by:

$$Q_{\text{in}} = \dot{m} \cdot (h_3 - h_2)$$

Referring more specifically to the subject of the thermo-structural analysis, the turbine comprises two main components: the stator and the rotor, which sequentially interact with the fluid flow, forming the turbine stages. The stator increases the tangential velocity of the gas to optimize the attack angle on the rotating blades, enhancing efficiency. Conversely, the rotor harnesses the expansion of hot gases to generate tangential thrust on the blades, thereby rotating the turbine rotor. The primary components for comparison between the two *Inconel* alloys will be the rotor discs, of which the FR1500 has three.

As shown in Figure 3, the rotor assembly includes several key elements: the Distance Piece, which maintains precise axial spacing and alignment between rotor components; Turbine Wheels 1, 2, and 3, which house the blade dovetails at their periphery, securing the rotating blades; Spacers 1 and 2 that alternate between the turbine wheels, providing necessary separation and thermal insulation; and the Afterward Shaft, which connects the rotor assembly to the generator or load, transmitting torque and supporting the overall mechanical structure. The picture represents half of the cross-section of the rotor assembly. The entirety of the rotor can be better visualised after a 360 degrees revolution around an horizontal axis beneath Figure 3.

Talking about the gas flow,in the picture it develops from left to right, approaching the first turbine wheel with the maximum temperature-energy. Typically, turbine wheels and spacers are constructed using Inconel alloys, which are the subjects of this analysis. Conversely, the distance piece is positioned longitudinally adjacent to the combustor, resulting in its exposure to lower temperatures. Also the afterward shaft, which is traversed by cooler exhaust gases, is also subject to lower thermal stresses. Therefore, these two components are generally fabricated from materials other than superalloys.

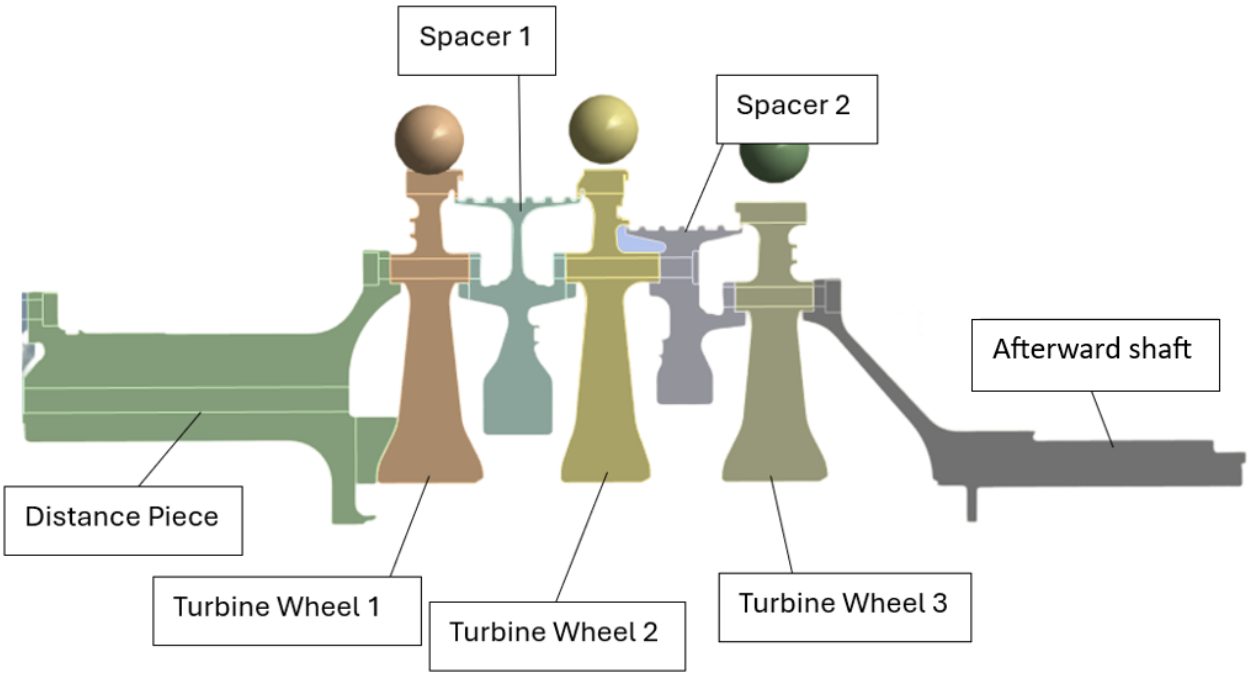

Figure 3: Components of a FR1500 rotor

Figure 3 illustrates three through-holes that connect each turbine wheel with the two adjacent components of the assembly. These holes accommodate tie rods, which are secured using bolts. The function of the tie rods is to fasten each component of the turbine system to the preceding and succeeding ones, thereby ensuring

compactness and coaxial alignment. These through-holes affect the mechanical properties of the turbine disks, necessitating adjustments in the ANSYS simulation model, as will be discussed subsequently. Furthermore, the contact areas near these tie rods, between spacers and turbine wheels, represent a critical feature in the development of the system mesh and the boundary conditions that must be set before initiating the Finite Element Analysis (FEA). This aspect will also be elaborated upon in the following sections.

To conclude, for the subsequent analysis it is necessary to introduce spacers and turbine wheels as components in more detail, highlighting some specific sections at slots or junctions. These sections will later be characterised by thermo-structural criticalities.

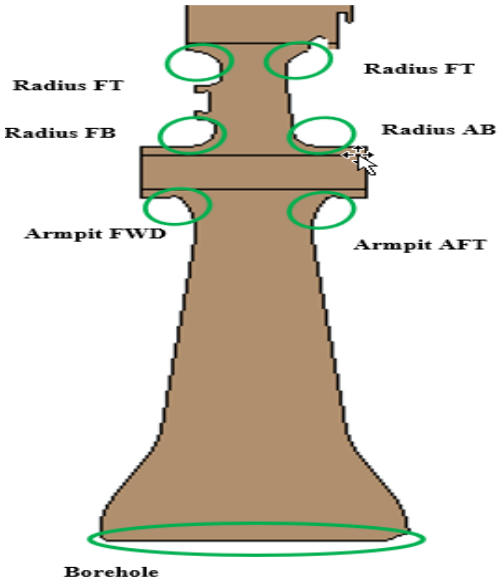

Figure 4: Turbine Wheel sections

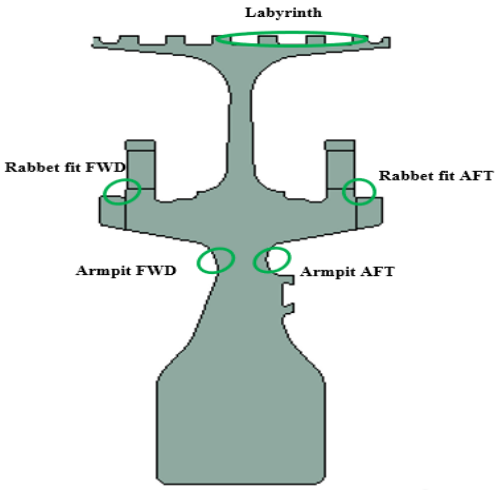

Figure 5: Spacer sections

2.2 Joule-Brayton Cycle

The Joule-Brayton cycle (Figure 6) is the cornerstone of gas turbine operation and represents a sequence of thermodynamic processes that facilitate the conversion of fuel into mechanical energy. In the ideal Joule-Brayton cycle, air undergoes isentropic compression in the compressor, constant-pressure heat addition in the combustor, isentropic expansion in the turbine, and constant-pressure heat rejection into the surroundings. This idealised cycle assumes perfect, reversible and lossless processes, thus achieving maximum theoretical efficiency.

However, as shown with the dotted line, real-world gas turbines operate under conditions that significantly deviate from this ideal model. In practical scenarios, the compression and expansion processes within the compressor and turbine are not perfectly isentropic. Instead, they exhibit polytropic behavior due to irreversibilities such as friction, mechanical losses, and heat transfer with the environment. These irreversibilities result in an increase in entropy, reducing the actual work output compared to the ideal case.

Moreover, the combustor introduces additional complexities. In an ideal Joule-Brayton cycle, heat is added at constant pressure, but in reality, pressure losses occur due to factors such as incomplete combustion, turbulence, and aerodynamic drag. These losses lead to a lower pressure at the turbine inlet, which in turn reduces the expansion work that the turbine can perform. The pressure drop across the combustor is a critical parameter that engineers strive to minimize through advanced combustor designs and optimized combustion techniques. To quantify these deviations, engineers use the concepts of isentropic efficiency for both the compressor and turbine, as well as combustor efficiency. Combustor's performances as well as the isentropic efficiency of the compressor and turbine (η_t) are defined as:

$$\eta_{n\pi c} = \frac{p_3'}{p_2}$$

$$\eta_c = \frac{\text{Isentropic Work Input}}{\text{Actual Work Input}}$$

$$\eta_t = \frac{\text{Actual Work Output}}{\text{Isentropic Work Output}}$$

These efficiencies account for the losses and provide a more accurate measure of performance. For instance, typical isentropic efficiencies for modern compressors and turbines range from 85% to 90% [**1**], reflecting the inherent inefficiencies.

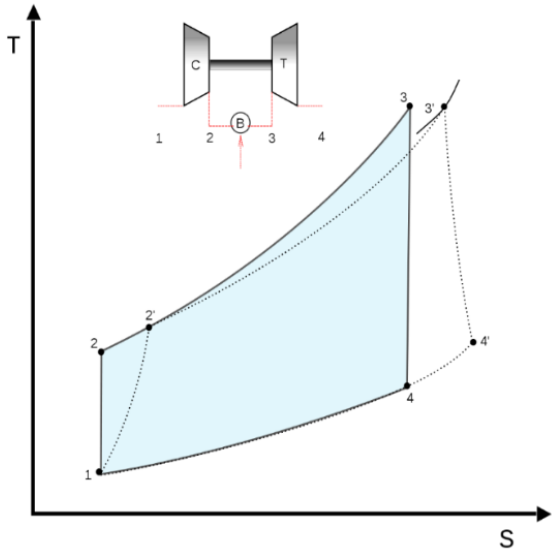

Figure 6: Joule Brayton cycle: ideal and real cases

The overall cycle efficiency is influenced by the pressure ratio β_p of the compressor and the turbine inlet temperature (T_3 or TIT). Higher pressure ratios and turbine inlet temperatures generally enhance the thermal efficiency of the cycle.
The useful work, L_u, depends on the values of T_3 and β:

$$L_u = \eta Q_1 = (1 - \frac{1}{\beta^{\frac{k-1}{k}}}) c_p T_1 (\frac{T_3}{T_1} - \beta^{\frac{k-1}{k}}) \tag{1}$$

Therefore, it is crucial to find a balance between the β that maximizes useful work ($\beta_{Lmax} = \beta_{\text{lim}} = 0.5$) and the temperature T_3 that the components can withstand. It is advisable to maximize the specific work to achieve the same power output using lower flow rates.

2.2.1 Turbine Inlet Temperature

This project particularly focuses on the Turbine Inlet Temperature because a higher T_3 -or TIT- increases the area enclosed by the cycle on the T-S diagram, thereby enhancing both the output power and efficiency. The reason is that high turbine inlet temperatures are indicative of efficient combustion processes within the combustor. Achieving and maintaining high T_3 values ensure that the fuel is utilized effectively, maximizing the energy conversion from chemical energy to thermal energy. Furthermore, higher T_3 values often result in increased NOx emissions, as nitrogen in the air reacts with oxygen at elevated temperatures [**2**]. This necessitates the use of emission control technologies such as dry low NOx (DLN) combustors to mitigate environmental impact.

However, the most important point in relationship with the future analysis is that it is crucial to ensure that the TIT is consistent with the material properties of the turbine components. Elevated TITs can lead to material failure and reduced performance due to thermal stress and creep. Consequently, optimizing the material selection for turbine wheels and disks is imperative to withstand high operating temperatures. As elaborated in the subsequent chapter, *Inconel* alloys, including NiCoCr alloy and NiCrFe alloy, typically maintain structural integrity up to approximately 900°C. Given that the TIT often exceeds this threshold, effective cooling strategies are essential.
The cooling of turbine components can be achieved through two primary methods:

1. *Convective Cooling or Film Coating:* This method involves the use of small nozzles on the external surface of the blades to create a thin film of cooling air. The cooling air is bled from the compressor and directed through these nozzles, forming a protective layer that insulates the blade from the hot gases. This technique not only reduces the blade temperature but also minimizes thermal gradients and associated thermal stresses. Convective cooling is particularly effective in maintaining the durability and performance of turbine blades under high-temperature conditions [**3**].

2. *Thermal Barrier Coatings (TBC):* This method employs a ceramic coating, typically applied to the surfaces of Turbine Wheels 1 and 2. The ceramic layer acts as an insulator, significantly reducing the heat transfer from the hot gases to the underlying metal. This coating allows the metal components to operate at lower temperatures despite the high TIT, thereby extending their lifespan and maintaining structural integrity. Thermal barrier coatings are essential in modern gas turbines to achieve higher TITs without compromising the material properties and overall reliability of the turbine.

3 Materials

3.1 NiCoCr alloy and NiCrFe alloy

NiCrFe alloy and NiCoCr alloy, both nickel-iron-based superalloys, are extensively utilized in high-performance applications such as aircraft turbines, rocket engines, and power generation turbines due to their remarkable mechanical properties. NiCrFe alloy is characterized by a higher percentage of alloying elements, including significant amounts of nickel and chromium, which confer excellent tensile strength and creep resistance at elevated temperatures. Moreover, has extremely high resilience, excellent tensile fracture resistance, and good corrosion resistance. However, this alloy presents considerable challenges in conventional machining, such as poor surface finish, low dimensional accuracy, and a high tool wear rate, primarily due to its high work-hardening tendency and abrasive nature. In contrast, NiCoCr alloy, a relatively newly developed superalloy, offers enhanced fabricability alongside high mechanical strength, making it particularly suitable for turbine disk applications. This alloy contains a lower percentage of alloying elements compared to NiCrFe alloy but includes both niobium and aluminum, contributing to its robust performance characteristics. NiCoCr alloy is often less expensive due to its easier manufacturing processes and reduced need for heat treatment. The high toughness of NiCoCr alloy ensures the absence of microcracks on the machined surface. Despite these advantages, NiCoCr alloy also faces difficulties in conventional machining, necessitating the use of Wire Electrical Discharge Machining (WEDM) to achieve better surface finish and dimensional accuracy [**4**]. However, these disadvantages mostly regard machining of the material, rarely influencing performances over operational cycles.

The slight differences between the two super-alloys can be noted by looking at their chemical compositions (Figure 7 and Figure 8):

Ni	Fe	Cr	Co	Mo	Nb	Ti	Al
40,98	Bal.	16,5	0,03	0,06	2,9	1,68	0,225
C	Mn	Cu	S	Si	V	P	Zr
0,017	0,08	0,01	0,00015	0,04	0,03	<0,005	0,006

Figure 7: NiCoCr alloy chemical composition

Ni	Cr	Co	Mo	Al	C
50–55	17–21	1 max	2.8–3.3	0.3–0.7	0.02–0.08
Si	Mn	Fe	Cu	S	P
0.35 max	0.35 max	rest	0.2 max	0.015 max	0.015 max
B	Nb + Ta	Ti			
0.006 max	4.8–5.5	0.7–1.15			

Figure 8: NiCrFe alloy chemical composition

Finally, before initiating the analysis, it is important to consider that rotor disks, like every component in a turbogas plant (in our case, the FR1500 turbine), must be guaranteed for a certain number of cycles if they operate under start-stop conditions, meaning through operational cycles of ignition and shutdown, or for a certain number of equivalent hours if they operate at full load, meaning continuously without stopping. The standard values for which the component must be guaranteed are 5,000 cycles and 144,000 equivalent hours, as these represent the average time after which maintenance is typically performed. This is the reason why materials selection plays a crucial role.

3.2 Differences between the two super-alloys

As previously mentioned, NiCoCr alloy exhibits superior mechanical strength compared to NiCrFe alloy. Figure 9 illustrates the Young's modulus of both materials at various operating temperatures. The temperature range to which the system is subjected during a turbogas cycle is extensive, and the thermal cycle is a crucial factor to consider. As evident from the graph, NiCoCr alloy consistently shows a higher Young's modulus across the temperature range. According to Hooke's Law it is rational to conclude that for a given stress, NiCoCr alloy will undergo less deformation compared to NiCrFe alloy. This implies that NiCoCr alloy is more resistant to deformation under the same loading conditions, making it a more desirable material for applications subjected to high mechanical stresses within a broad thermal range.

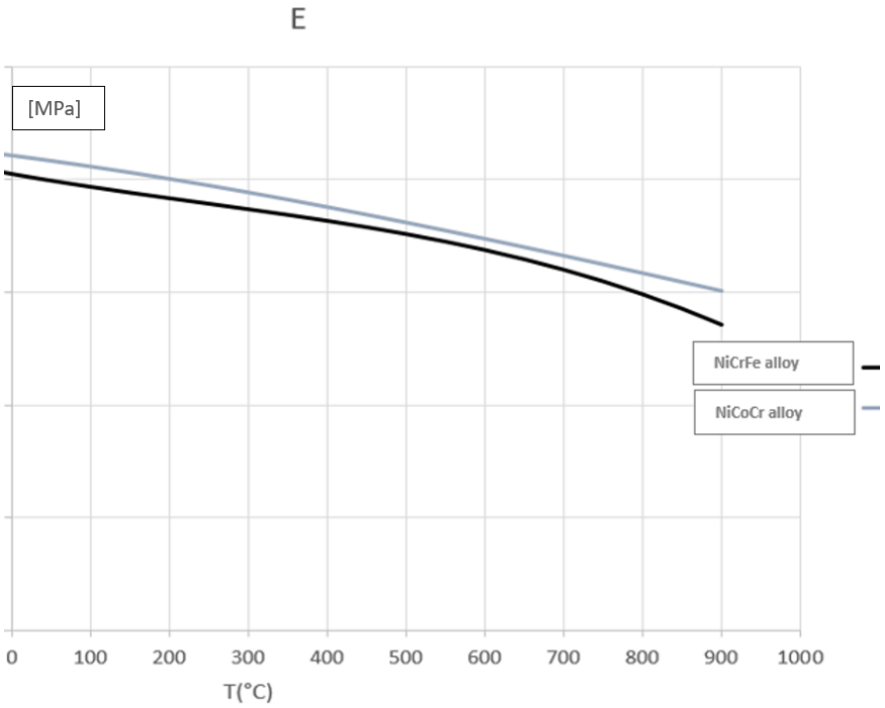

Figure 9: NiCrFe alloy and NiCoCr alloy Young's Module comparison

Another important property of the two materials is their minimum ultimate tensile strength S_y, which is the minimum stress at a defined temperature at which the material fails under tensile loading. For the two alloys, it is possible to refer to the following graph. This graph is based on experimental data from tests conducted internally at EthosEnergy. For this reason, the stress values on the abscissa have been normalized with respect to the S_y of NiCrFe alloy at ambient temperature (20°C).
It is important to note that all reported characteristics regard the longitudinal/transverse direction relative to the fibers, as these values are lower than those along the longitudinal direction. The choice to refer to the minimum ultimate tensile strength, and not the average ultimate tensile strength, is a conservative engineering approach that increases the safety factor during the design phase and allows for the examination of the worst-case scenario during component verification.

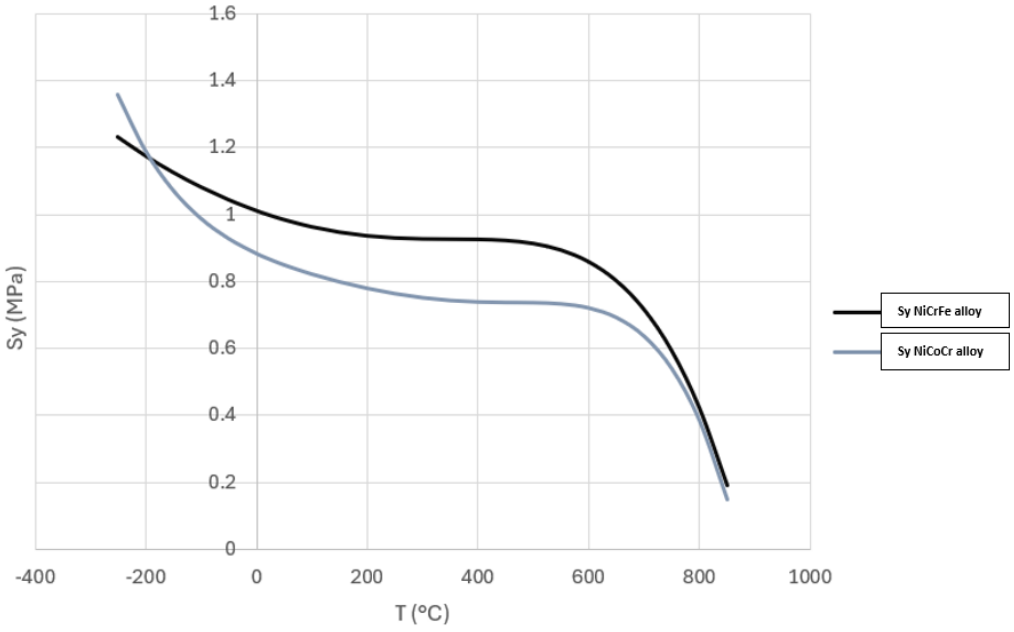

Figure 10: Minimum Ultimate Tensile Strenght comparison

As shown in Figure 10, NiCrFe alloy offers better tensile strength compared to NiCoCr alloy, especially at high temperatures. Despite this, NiCoCr alloy remains mechanically stronger and more workable, as previously discussed. For a turbine disk, axial stress, meaning the stress experienced in a parallel to the axis of rotation direction, is not the only stress encountered. It is mainly caused by axial material deformations due to high temperatures.

However, the most critical stress is the radial one because it results from the centrifugal forces acting on the disk during high-speed rotation. These forces create a significant radial stress, which can cause the material to expand outward from the center, potentially leading to deformation or failure if not adequately managed. Additionally, the disk also experiences tangential (hoop) stress, which is the stress acting perpendicular to the radius, around the circumference of the disk. This stress is a consequence of the material's resistance to being pulled apart by the centrifugal force. In summary, ANSYS analysis showed that while axial stress is significant, the radial stresses are more critical for the FR1500, possibly due to the intense centrifugal forces encountered during operation.

Although the two alloys are similar, they exhibit various substantial differences when studied under operational conditions. This study aims to investigate the behavior of the two alloys in rotor disks during operation (from start to stop). To achieve this, before initiating the simulation in ANSYS to compare the thermo-structural results, we will hypothesize, through a comparison between the two materials, how they will behave with respect to the main causes of failure. The primary causes of failure include creep, or viscous deformation, membrane stress related to the average primary allowable stress, and low cycle fatigue (associated with the Smith-Watson-Topper (SWT) stress).

3.2.1 Creep and Membrane Stress

As mentioned, membrane stress and creep are two of the main causes of failure for a component in a gas turbine plant. Membrane stress refers to the in-plane stress within a structural element, such as a shell or plate, which resists external loads primarily through tensile or compressive forces rather than bending. This type of stress is crucial in analyzing the structural integrity of turbine disks and other components subjected to high rotational speeds. Membrane stress varies with the shaft rotational speed, as well as with thermal loads of the system. However, EthosEnergy engineers focus on membrane stress only when related to rotational speed. For this reasons, the red lines of the following graphs refer to a situation of the system without thermal stresses, but with nominal rotational speed of the shaft. This situation is precisely the end of the ramp-up state of the motor, where it reaches nominal speed, even if the temperatures of the components are still not that high. This time of the operational cycle of the turbine, corresponding to the end of the ramp-up transitory state, is the one of reference for membrane stress future comments.

Creep, or viscous flow, is on the other hand the slow and permanent deformation of a material subjected to a constant load over a long period. This phenomenon is particularly relevant at high temperatures and in materials subject to mechanical stresses, such as metals and alloys used in high-temperature applications. Therefore, it is possible to represent both causes in a single diagram as a function of temperature for both materials analyzed (Figure 11 and Figure 12).

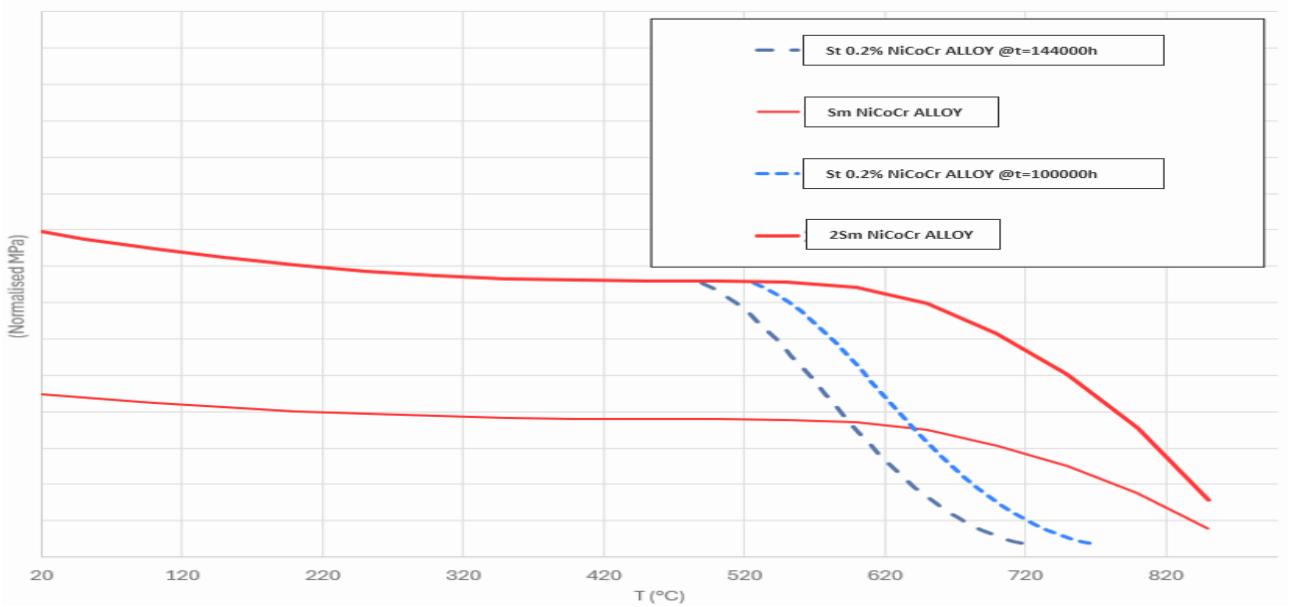

Figure 11: Primary admissible membrane stress NiCoCr alloy

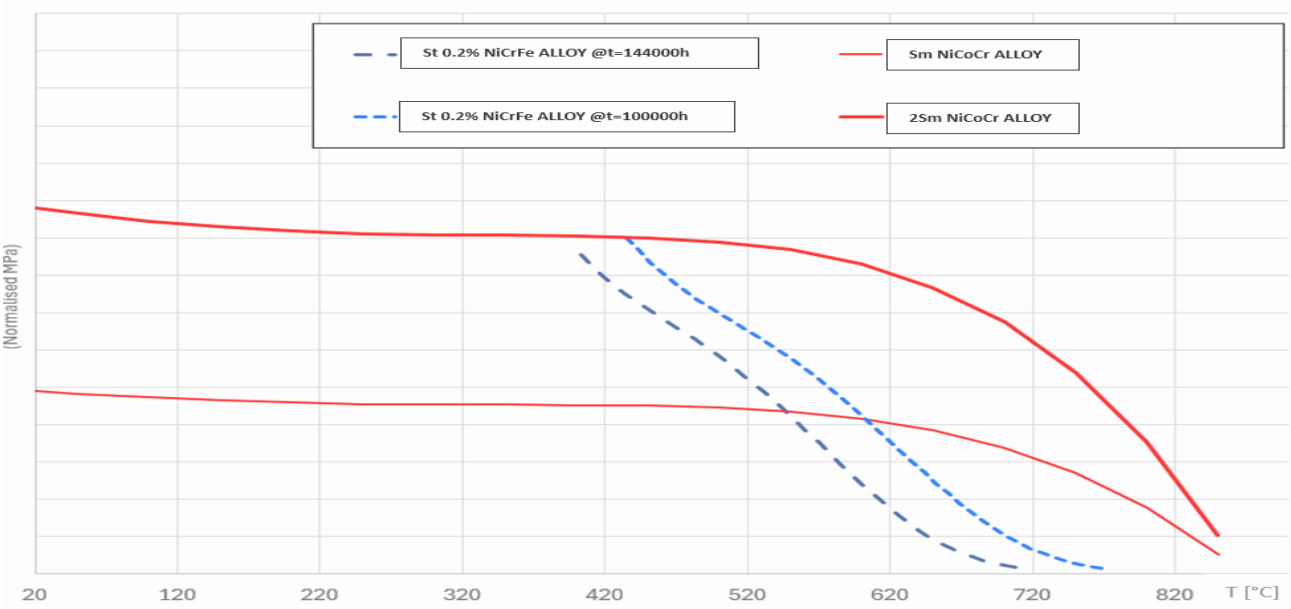

Figure 12: Primary admissible membrane stress NiCrFe alloy

The x-axis and y-axis along with the explanation of the curves... On the graph, it is possible to represent a physical point of a component in operation at a certain temperature. To represent the point, reference should be made to the local elementary von Mises stress, which ANSYS will calculate for each point of the assembly following the simulation.

To verify the part, it must be ensured that the operating point is within the area under the curves and not above them. Specifically, if the operating point is to the left of the dashed curves, it indicates that the part has been verified for creep for a certain number of equivalent operating hours. If the point is below the solid curve, it means that the analyzed point is sustaining a membrane stress lower than the critical stress. In reality, the choice to illustrate S_m and not $2S_m$ and S_t 0.2% is very conservative. Therefore, if the point falls slightly above the area covered by the graph, it does not necessarily mean that the component is definitively unverified; rather, it means that it will need to undergo further assessments, such as through 3D simulations exclusively concerning the problematic component.

One of the objectives of the subsequent analysis is to plot the operating points of the components on the diagrams for both materials. This operation aims to qualitatively observe how close the components of a given material approach failure during operation and, in an initial analysis, conclude which material is better for each of the components that make up the turbine rotor assembly. Specifically, this check gives information about potential failures linked to creep phenom and excessive membrane stresses.

3.2.2 Smith-Watson-Topper stress and Low Cycle Fatigue

The Smith-Watson-Topper (SWT) parameter is a critical tool in the analysis of Low Cycle Fatigue (LCF). This parameter is particularly useful because it provides a robust measure for predicting the fatigue life of materials under cyclic loading conditions, where significant plastic deformations occur. The SWT parameter combines the maximum stress and strain experienced by the material into a single parameter, thus effectively capturing the complex interactions between stress and strain that drive fatigue damage in the low cycle regime. By considering both the elastic and plastic components of strain, the SWT parameter allows EthosEnergy engineers to more accurately assess the durability and performance of materials subjected to high-strain amplitudes. In the case of EthosEnergy, a minimum Smith-Watson-Topper tension is calculated, based on the worst-case scenario. This approach is taken to incorporate conservatism, thereby ensuring a higher safety factor.

What follows is a Smith-Watson-Topper diagram about the two analysed materials.

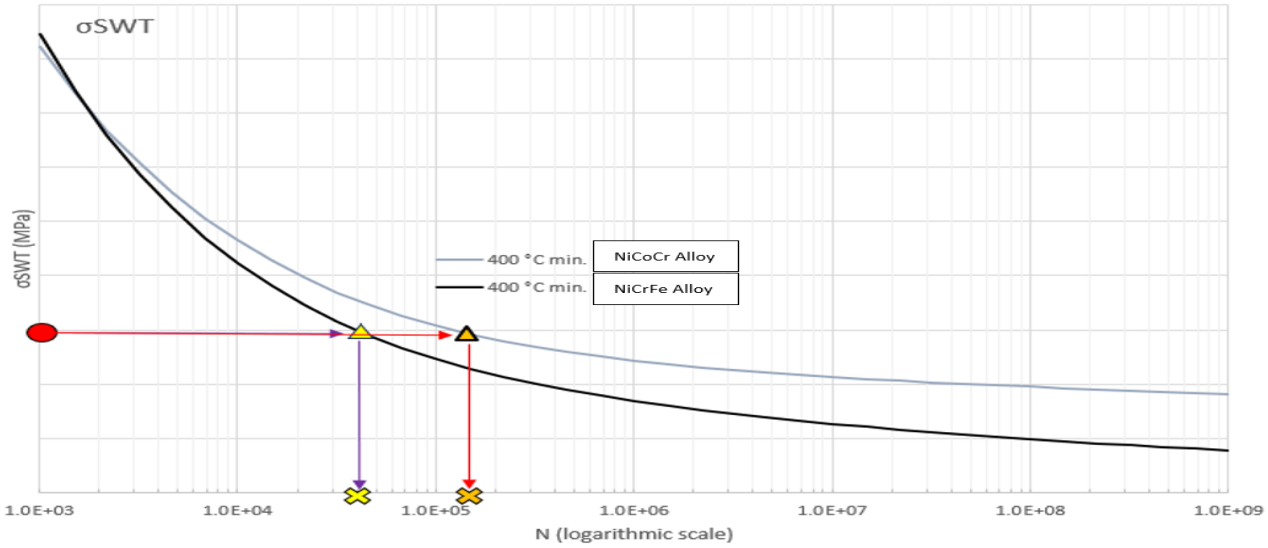

Figure 13: Low Cycle Fatigue (LCF) Diagram

The lighter curve represents NiCoCr alloy, while the other represents NiCrFe alloy. These curves rise and fall in relation to temperature and the number of cycles being evaluated —*in the proposed analys 5,000 operational cycles*— according to an internal company algorithm. For this purpose, the ordinates have been normalized to ensure confidentiality.

The graph represents the Smith-Watson-Topper (SWT) stress on the ordinates, or maximum equivalent stress, derived from the ANSYS analysis, and the number of cycles to failure on the abscissae. The graph can be interpreted in both directions.

The marks on the graph indicate an example reading at a given stress (red circle) for both materials. Starting from the stress value, move to the right until reaching the limit curve, then move downward to observe the number of cycles sustainable at that temperature. In this example, the two materials are compared at *400* degrees Celsius, which is a realistic temperature based on the ANSYS simulation. This qualitative example does not provide information on the LCF verification but demonstrates how, at the same temperature, the NiCrFe alloy curve is positioned lower than the NiCoCr alloy curve. From this, we can infer that the former material has a lower fatigue resistance in general.

Regarding the LCF verification proposed in this thesis, it is structured through several steps, which utilize the Smith-Watson-Topper diagrams. For the low cycle fatigue verification, the most critical area of each

component—for instance the borehole of a turbine—will be verified at 5,000 operational cycles. The reason for selecting ***N=5000*** operational cycles is that company policy requires maintenance interventions every 5,000 cycles or multiples thereof. The necessary steps to achieve this are as follows:

- Firstly deduce from the analysis the point where the maximum Smith-Watson-Topper stress is recorded, specific to a particular area of each rotor assembly component. It is also useful to note the moment—referred to as t_peak—when this maximum point is recorded for each component during the entire analysis. This allows understanding not only where but also when each component experiences the maximum principal stress (or Smith-Watson-Topper stress).
- Record the maximum principal stress and the temperature at the most critical point for each component.
- Then extrapolate the equivalent number of cycles that would lead to failure using the Smith-Watson-Topper graph. This quantity is identified by n.
- **4.** Finally, divide this value by the number of cycles to be verified to obtain a percentage value that indicates how close the component is to failure and how often it as to be inspected for maintenance purposes. For example, if N/n *[%]* equals 50%, it means that the component can theoretically be inspected every two maintenance cycles.

4 ANSYS analysis

The simulation was conducted following a previous Computational Fluid Dynamics (CFD) analysis performed internally within the company, in addition to transient curves during start-up and shutdown derived from real engine operational cycles. This CFD analysis provided the temperature and pressure profiles, fluid velocities, and the necessary coefficients required for the subsequent thermo-structural analysis.The latter consists of two separate steps supported by ANSYS Mechanical.

1. *Transient Thermal Analysis* involves the simulation of temperature distribution and heat flow in a component or system over time, considering the effects of time-dependent thermal loads and boundary conditions. This analysis is essential for understanding the thermal response of materials and structures when subjected to varying thermal environments.

   In the context of the FR1500 gas turbine rotor, the transient thermal analysis begins with the definition of the initial temperature distribution of the flowing gasses and the application of time-varying thermal loads, such as convection, radiation, and heat generation. The governing heat conduction equations are solved using finite element methods to obtain the temperature distribution at discrete time intervals. This approach allows for the assessment of thermal gradients, thermal stresses, and potential thermal fatigue over the operational cycle of the turbine. Accurate transient thermal analysis is critical for predicting the thermal behavior of turbine components under realistic operating conditions and provinding data about the thermal stresses, necessary to solve for the Static Structural model.

2. *Static Structural Analysis* concerns the evaluation of the mechanical response of a structure under static loading conditions to determine stress, strain, and displacement distributions. This type of analysis is fundamental for ensuring the structural integrity and safety of engineering components, such as the rotor disks in the FR1500 gas turbine.

   The process begins with the definition of material properties, geometric models, and boundary conditions. External loads, including forces, pressures, and thermal loads (derived from the transient thermal analysis), are applied to the model. The finite element method is employed to solve the equilibrium equations, resulting in the computation of stress and deformation fields. The analysis provides insights into the maximum stress locations, deformation magnitudes, and potential failure points. It is crucial for verifying that the turbine components can withstand operational loads without yielding or failing, thus ensuring reliable and safe operation. The Static Structural model is solved with just the Isotropic Elasticity material model, which requires two property values: Young's Modulus and Poisson's Ratio. This assumption is only correct if the material is isotropic, but all the turbine rotor components are assumed to satisfy this condition.

   In particular, the main areas of interest of the analysis for stress fields are the most critical ones, such as Rabbet fit radius, Borehole, *SP1-2* Labyrinth section and TW3 Armpits.

All the analysis were performed in 2D, since the components of interest -turbine wheels, spacers, distance piece and afterward shaft- are axisymmetric. Thus, after adding some apposite boundary conditions, the solution can be revolved around the axis of symmetry to obtain the 3D solution.

4.1 Neuber's Law

Neuber's Law will be used to convert post-processed output tensions by ANSYS to real and correct local tensions values. This is because ANSYS Mechanical does not account for the plasticity of materials but rather considers only their elasticity.
Consequently, the stress-strain diagram of a material, according to ANSYS, is a straight line originating from the origin with a slope corresponding to the elastic portion. Therefore, if the yield point is exceeded and the material begins to deform plastically, it is important to be aware that ANSYS will subsequently provide erroneous stress values after the simulation. For significant deformations, the software will incorrectly treat the point as if it were still deforming elastically.

In ANSYS, once the material enters the plastic deformation region, the linear elastic assumptions used by the software are no longer valid. This means that the stress values reported by the simulation will not accurately reflect the true stress state of the material. Instead, the software will continue to assume an elastic response, leading to incorrect stress calculations.

To correct this issue, it is possible, where necessary, to calculate the elasto-plastic stress using Neuber's rule [**6**]. Neuber's rule is a method used to estimate the stress and strain in a material that has undergone plastic deformation. It accounts for both elastic and plastic components and provides a more accurate representation of the stress state.

Neuber's rule states that the product of the elastic stress and strain concentration factors is equal to the product of the actual (elasto-plastic) stress and strain. This relationship can be expressed mathematically as:

$$\frac{Kt^2 \cdot S \cdot e}{\epsilon} = \sigma$$

where:

- Kt is the theoretical stress concentration factor
- ϵ is the local strain and e is the nominal strain
- σ is the local stress and S is the nominal stress

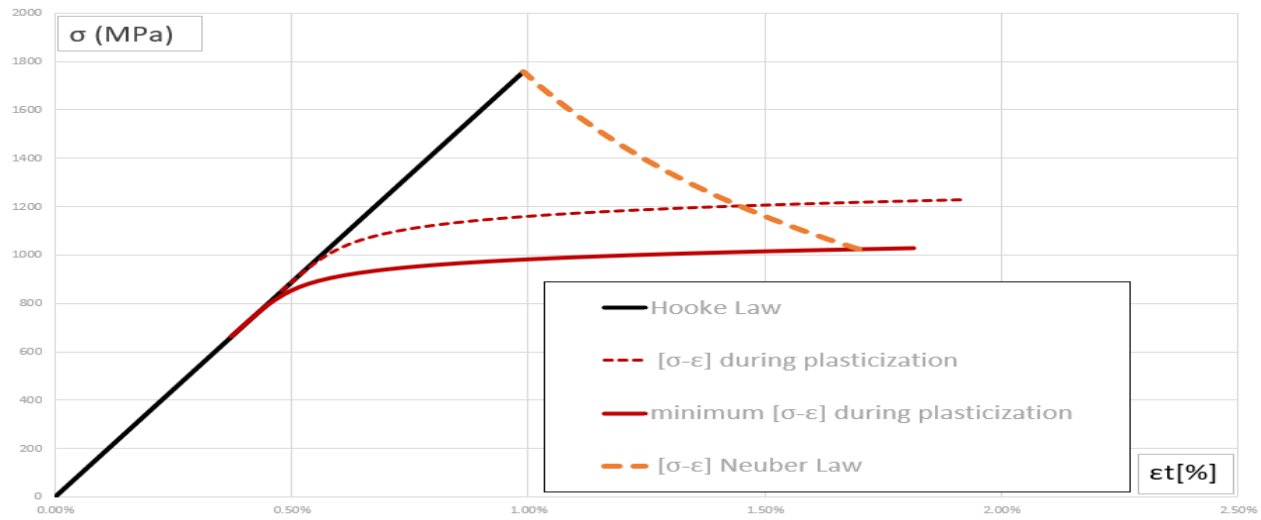

Figure 14: Qualitative illustration of Neuber's Law

4.2 Boundary conditions and used features

Setting boundary conditions in this context is crucial for accurately simulating the physical behavior of the turbine components under operational conditions. The most influential boundary condition choices will be explained below.

The mesh differences, particularly in areas like the contact between spacers and turbine wheels, necessitate a more detailed mesh to ensure accuracy in the analysis. This is because contact regions typically experience high-stress concentrations and complex interactions that require a finer mesh to capture the gradients and variations accurately. This is the reason why the All Triangles Method mesh [**7**] has been selected, with single element size ranging from $10mm$ to a $3mm$ element size in more critical areas. A detailed mesh in these areas allows for better resolution of the physical phenomena, leading to more accurate predictions of stress distributions, potential wear, and failure points. Other areas that require a finer mesh are at the notches and fillets of the spacers and wheels geometry, as in these zones, according to theory, the stress will be multiplied by the stress concentration factor and consequently will be increased. Finally, a static friction condition must be set between the male-female disc interfaces because, in the FR1500 turbine, each rotor disk is connected to the next through a male-female system. There is no splined shaft that mechanically connects all the disks, around which the disks would behave as a hub. Instead, in the FR1500, each disk acts as a shaft for the subsequent disk and as a hub for the previous one, interlocking to ensure fixation by friction.

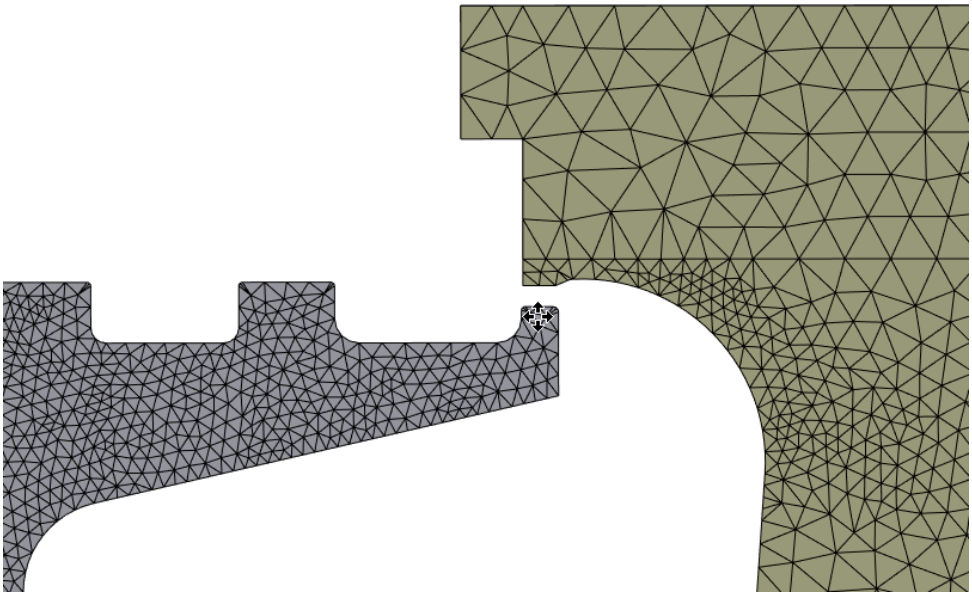

Figure 15: Mesh model

The analysis is conducted as a 2D transient analysis, which is then rotated 360 degrees to obtain the solutions, assuming axisymmetry. Simulating components in 2D reduces computational complexity compared to 3D, facilitating faster analysis of stress and thermal gradients. This efficiency allows for quicker turnaround times in simulations. Nevertheless, some patterns of the geometry do not satisfy axysimmetry. On major example are turbine disks' cavities -*or veins*-; they cannot be revolved due to their irregular shape. Therefore, a plane stress condition must be applied. By applying a plane stress condition, the analysis will assume that stresses vary significantly only within the plane of the cavity cross-section. This assumption implies that stresses in the thickness direction (normal to the plane) are negligible or can be approximated as such for the purposes of the simulation.

Another important feature is orthotropic stiffness, which is employed for the through-holes of the turbine wheels intended for the tie rods. This involves an Excel implementation to calculate an area ratio average, which is then used to weight the Young's modulus accordingly. This implementation has been utilized to compute a fictitious Young's modulus, lower than the actual one, specifically for the circular crown of the disk containing the through-holes. The adjustment is critical because, in that circular crown, the disk is not solid, and thus the material properties are negatively affected due to the presence of notches and concentrated stresses.
Furthermore, it is important to recall that our simulation is 2D, as previously mentioned. If we were to revolve our disk by 360 degrees, the simulation would perceive the disk as solid. Therefore, it is essential to assign a different material, with slightly degraded properties determined through the orthotropic stiffness calculus, at the locations of the through-holes.

The following steps outline this process:

1. *Area Ratio Calculation:* The actual cross-sectional area of the disk, including the through-holes, is compared to the cross-sectional area of an idealized solid disk. This ratio represents the reduction in effective material due to the presence of the holes.

2. *Weighted Young's Modulus:* The calculated area ratio is used to adjust the Young's modulus, resulting in a fictitious, reduced Young's modulus that more accurately represents the stiffness of the perforated section of the disk.

3. *Orthotropic Material Properties:* The orthotropic stiffness properties are then applied to these sections in the simulation model to reflect the anisotropic behavior caused by the through-holes. This ensures that the simulation accurately captures the reduced stiffness and increased susceptibility to stress concentrations in these areas.

5 Result of ANSYS analysis

5.1 Temperatures

The following are the temperature profiles at four different moments during operation, divided in two columns for NiCrFe alloy (Figures 16, 18 and 20) and NiCoCr alloy (Figures 17, 19 and 21) materials, respectively. These profiles have been normalized with respect to the maximum temperature recorded in the simulations of both materials. The highest temperature was observed for a component made of NiCrFe alloy, specifically at the labyrinth of the *Spacer 1-2*.

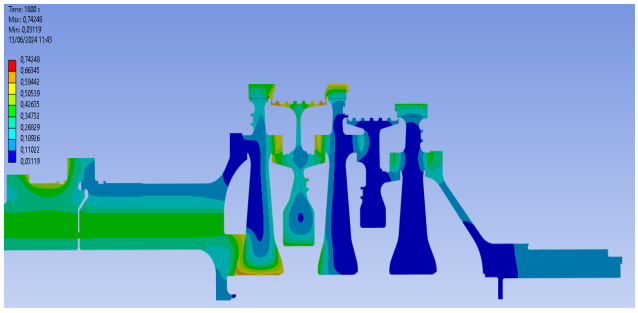

Figure 16: NiCrFe alloy - just reached full load at t=30min

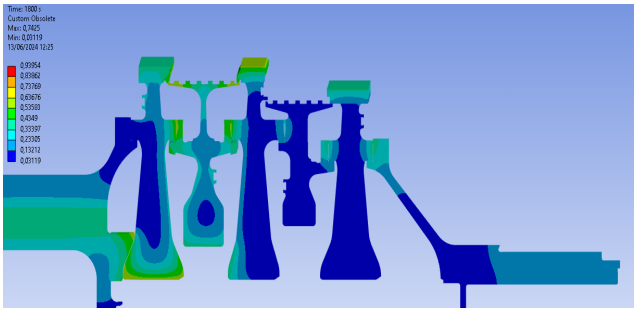

Figure 17: NiCoCr alloy - just reached full load at t=30min

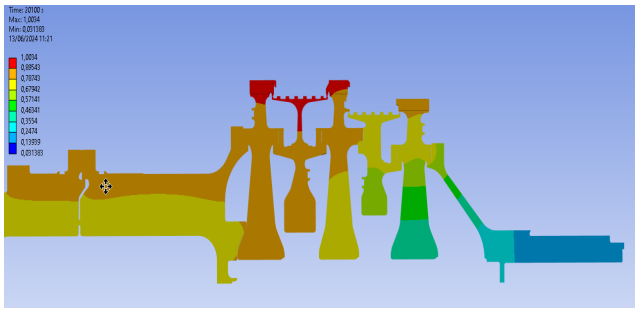

Figure 18: NiCrFe alloy - t=335min

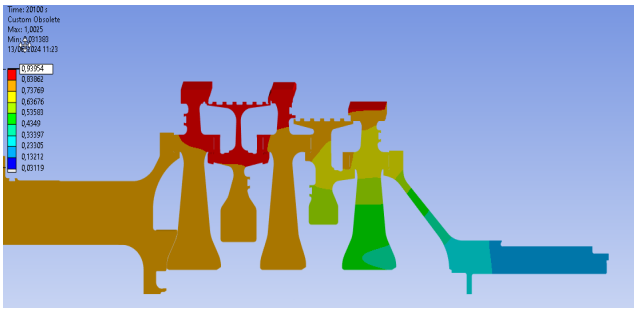

Figure 19: NiCoCr alloy - t=335min

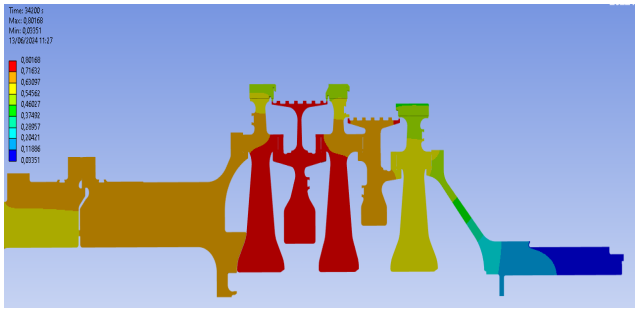

Figure 20: NiCrFe alloy: After ramp down

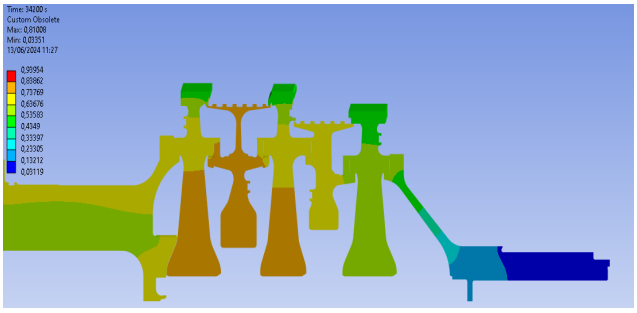

Figure 21: NiCoCr alloy: After ramp down

As can be seen graphically from the figure, a general trend for NiCoCr alloy is that it heats up less. For instance, at full exercise - *t=335 min* - the maximum temperature registered in the assembly made of NiCoCr alloy is only 0.93, as shown in Figure 19. Therefore, throughout the entire thermo-structural cycle, the temperature reached by the turbine disks and other components of the turbine rotor will be lower. However, this does not convey much structurally, because the absolute temperature alone does not provide meaningful information unless it is compared with the material's characteristics.

5.2 Radial deformations

Radial deformation in the rotor of a gas turbine is primarily caused by the high rotational speeds and the thermal expansion due to the elevated temperatures experienced during operation [**8**]. Axial deformation, on the other hand, is typically induced by thermal gradients along the length of the rotor and the differential expansion between various components. While both deformations pose significant risks, the thesis will only assess radial deformations.
The ANSYS analysis has shown that deformation mostly manifests in the disks and spacers of the rotor assembly, where the differential thermal expansion can lead to inexact alignments of the system, and so decreased performances. These stresses can also result in fatigue and creep, potentially leading to premature failure of the components. Additionally, excessive deformation creates an increase in pressures -and so stresses- at the contact points between the components.Moreover, although minimal, radial deformation also opposes the available area through which the fluid flows—parallel to the rotor axis—potentially affecting the turbine's efficiency.

At an operational time of approximately 20100 seconds, as seen in the previous section, the system reaches its maximum temperatures for both materials. Concurrently, the system also experiences the maximum radial deformations, which are illustrated below for the NiCrFe alloy. The values have been normalized relative to the maximum deformation experienced, as shown in Figure 22 and Figure 32.

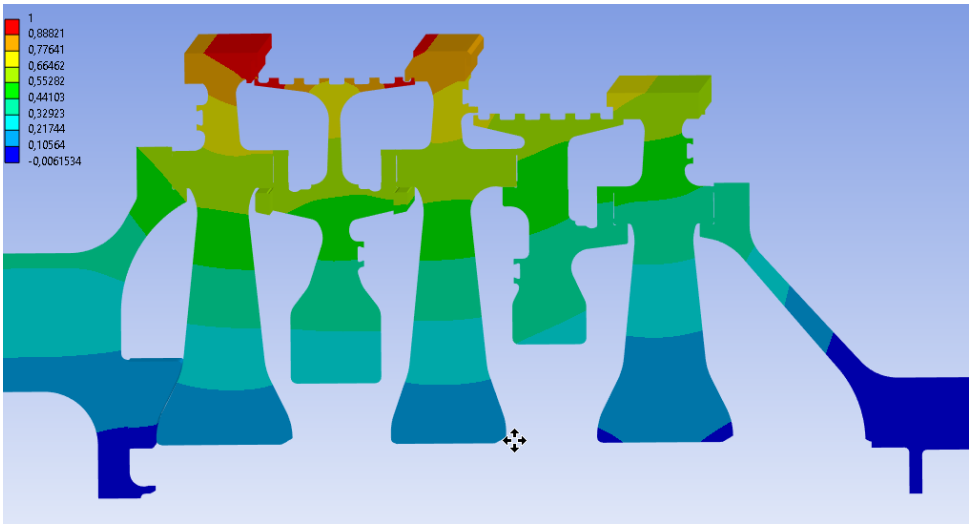

Figure 22: Rotor assembly radial deformation, NiCrFe alloy

It is evident that the main radial deformations occur at the labyrinth seals of Spacer 1-2 and the top of turbine wheel 1, the area closest to the gas flow—recalling that the latter flows from left to right. Below are representations of the individual parts:

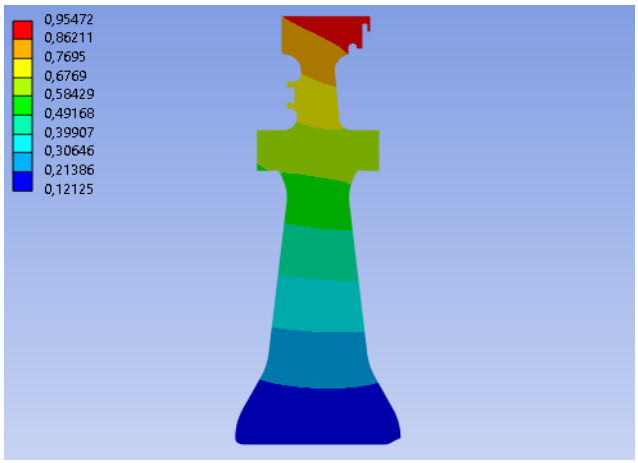

Figure 23: Peak radial deformation of TW1, NiCrFe alloy

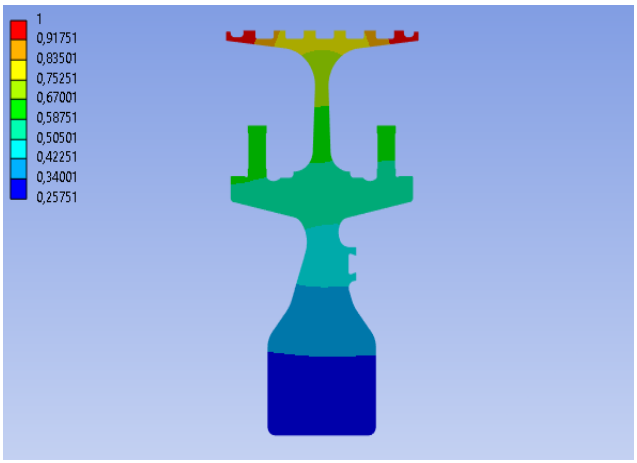

Figure 24: Peak radial deformation of SP1-2, NiCrFe alloy

After performing a similar analysis for the NiCoCr alloy, the results remained nearly identical. The maximum radial deformation recorded differs between the two materials by an order of tens of millimeters, and for the NiCoCr alloy as well, the maximum deformation occurs in the labyrinth of *Spacer1-2*.
In conclusion, although the radial deformation for both the NiCrFe alloy and the NiCoCr alloy is critical in determining the operational efficiency and structural integrity of the turbine rotor assembly, for the purposes of comparing the two alloys, the differences are so minimal that the two materials have been approximated as analogous in this regard. Therefore, the radial deformation did not actively influence the decision regarding which alloy will be considered superior.

5.3 Membrane stress and creep verification

For the following chapter, the general discussion will implicitly refer to both alloys. The distinction will only become apparent at the end, where the operating points of each component constituting the rotor assembly will be plotted on the diagrams related to creep and membrane stress *-3.2.1-*. This operation will, of course, be repeated for both materials to account for the different limit curves.

From the same chapter *-3.2.1-*, it is important to recall that the membrane stress depends on centrifugal forces and should ideally be calculated in the absence of thermal stresses [**9**]. However, during operation, thermal stresses are present; thus, it is chosen to consider the moment when the speed is at its operational value but the thermal stresses are minimal. The ideal moment when this occurs is at the end of the engine ramp-up, at $t^* = 1020$ *seconds* in the case of an FR1500 turbine, when the system begins to operate and the transient phase ends. Only in this way will the limit curves in Figure 11 and Figure 12 be valid.

The stress reported on the diagrams is the equivalent Von Mises stress, obtained by averaging a finite number of points on the section of each component. Therefore, with Ansys, multiple stress-temperature pairs were derived at various points of each component, all at t* = 1020 seconds. After identifying a "worst-case path" containing the critical point pairs of each component, these were averaged to represent each component (e.g., turbine wheel 1) with a single point on the graphs.

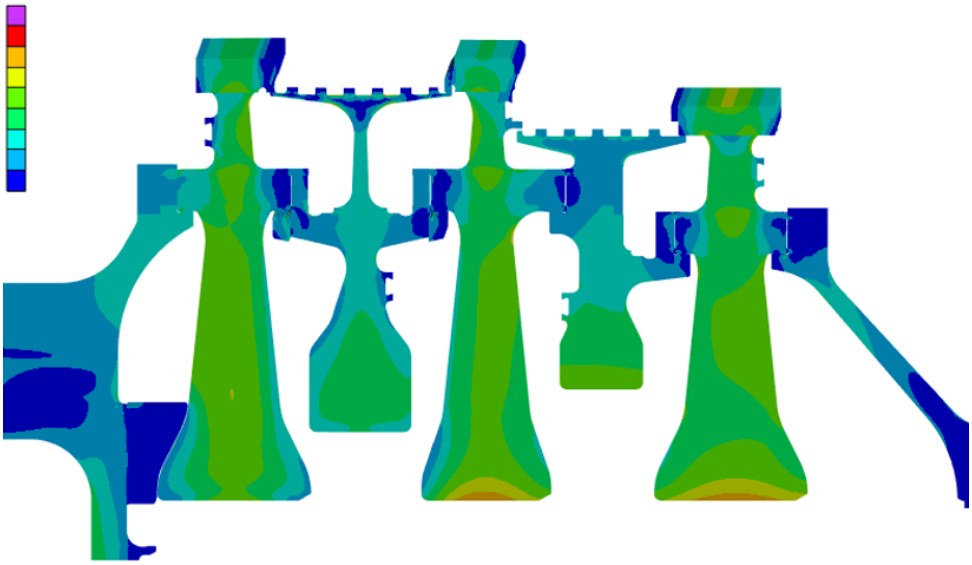

Figure 25: Overview of EvM distribution at $t*$ [Mpa]

By plotting the points on the graphs:

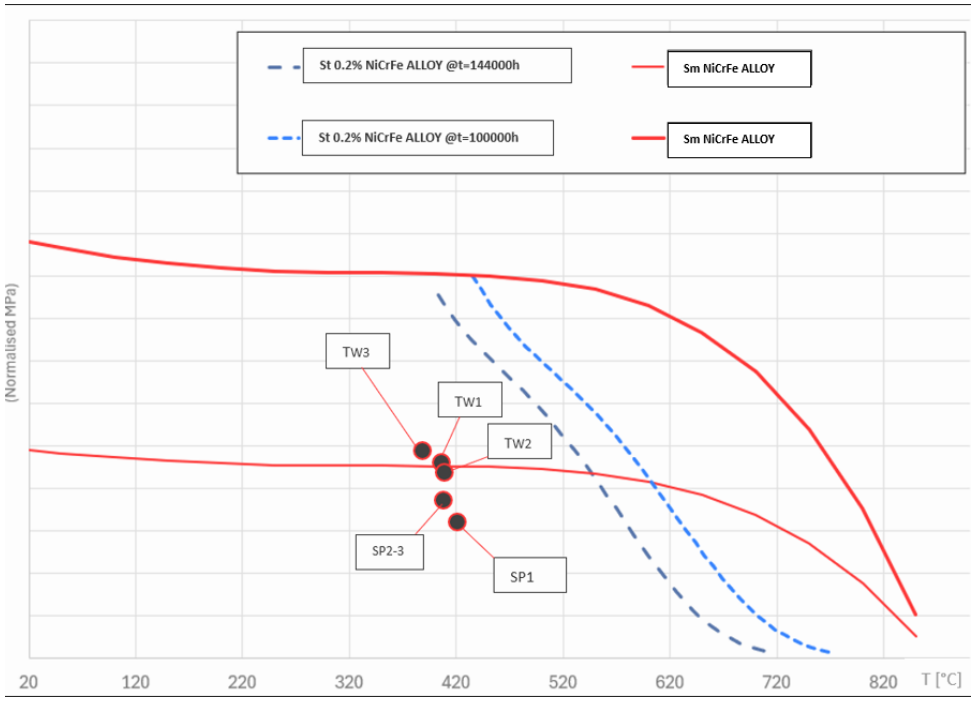

Figure 26: NiCrFe EvM distribution at $t*$ [Mpa]

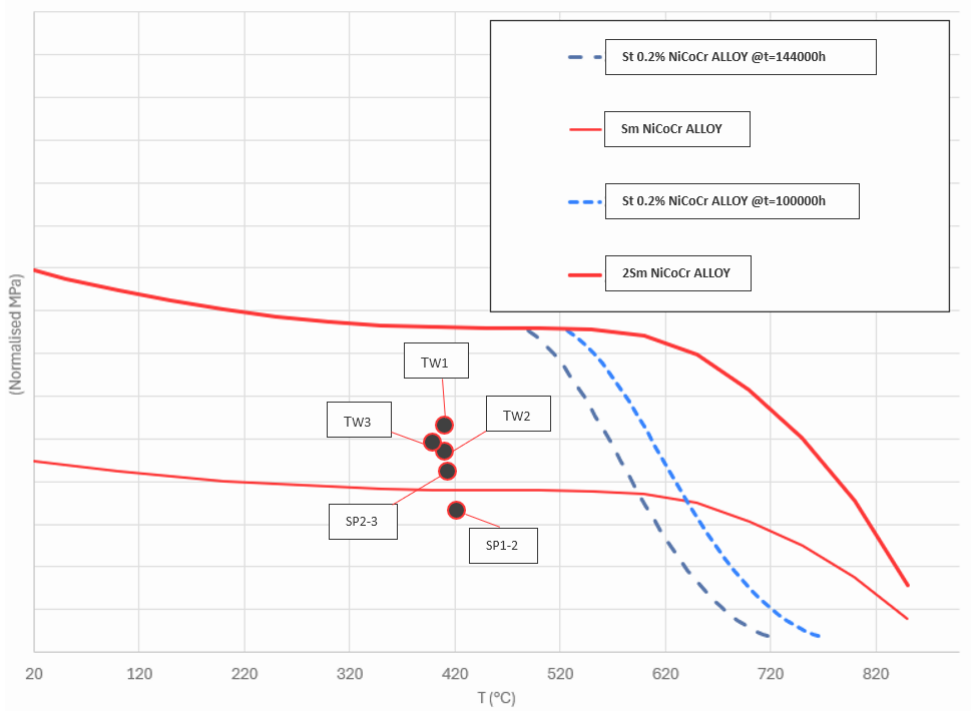

Figure 27: NiCoCr EvM distribution at $t*$ [Mpa]

As can be qualitatively observed, the points related to the NiCrFe alloy are located further below the limit curves. Therefore, this material performs noticeably better than the NiCoCr alloy.

5.3.1 Local problems

However, by analyzing the critical points of each individual component, it became evident that certain areas are sometimes subjected to von Mises stresses significantly higher than the average stress of the entire piece. These points could be at great risk. Here are three examples for turbine wheel 3, which is the most critical, as

shown below.

Three photos of turbine wheel 3 are provided as examples. As shown, certain areas of turbine wheel 3, including the fillet radii AB and FT and its borehole, are colored in red. This indicates that the limit curve for membrane stress has been exceeded. This observation applies to both materials analyzed.

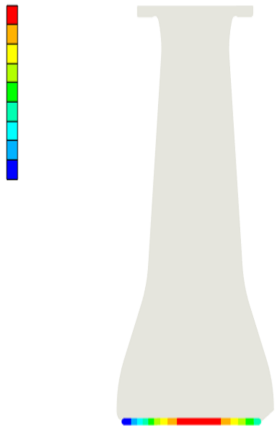

Figure 28: TW3 Borehole EvM at $t*$ [Mpa]

Figure 29: TW3 Radius AB EvM at $t*$ [Mpa]

Figure 30: TW3 Radius FT EvM at $t*$ [Mpa]

For this reason, a 3D steady-state analysis is suggested to better evaluate the risks.

5.4 LCF verification results

By performing the LCF analysis described in ***Chapter 3.2.2: Smith-Watson-Topper stress and Low Cycle Fatigue***, the following values are reported for the most critical area of each component of the rotor assembly for both materials. The exact values of temperature and stresses are normalized with respect to the highest value in each table.

Component	Region	t_peak [s]	T [°C]	σSWT norm[	n [n° cycles]	N [n°cycles]	N/n [%]
TW1	borehole	20580	0.81	0.87	9620	5000	52%
TW2	borehole	7200	0.71	0.80	13400	5000	37%
TW3	borehole	10800	0.31	1.00	7650	5000	65%
SP1-2	labyrinth	3600	1.00	0.79	13315	5000	38%
SP2-3	borehole	9000	0.31	0.95	9220	5000	54%

Figure 31: LCF NiCrFe alloy

Component	Region	t_peak [s]	T [°C]	σSWT [MPa]	n [n° cycles]	N [n°cycles]	N/n [%]
TW1	radius AT	5400	0.87	0.92	8410	5000	59%
TW2	borehole	10200	0.83	0.81	10100	5000	50%
TW3	radius FB	5400	0.57	1.00	5830	5000	86%
SP1-2	labyrinth	3600	1.00	0.96	6570	5000	76%
SP2-3	borehole	8500	0.29	0.94	11130	5000	45%

Figure 32: LCF NiCoCr alloy

As can be observed by comparing the two tables, in the case of the NiCrFe alloy, the percentages are less close to 100%, which, as previously mentioned, represents the threshold beyond which the component risks failing due to fatigue before the nominal inspection cycle, set at 5,000 cycles.

It can therefore be concluded that the NiCrFe alloy exhibits better fatigue resistance compared to the NiCoCr alloy. However, the analysis suggests that neither alloy has components exceeding the 100% threshold, and thus, a complete rotor assembly should withstand 5,000 operational cycles for both alloys. Nevertheless, it is recommended to conduct further analyses, such as 3D steady-state simulations, on the most at-risk components (TW3 and Spacer1-2).

6 Conclusions and Future works

All in all, the results indicate that NiCrFe alloy exhibits slightly superior performance at elevated temperatures compared to NiCoCr alloy. In terms of resistance to creep and stress membrane, it has been shown that the same components of the rotor assembly, operating under the same conditions, will be slightly less at risk if made of NiCrFe alloy. This holds true also for fatigue at elevated temperatures. These findings suggest that NiCrFe alloy could be a more suitable material for turbine rotor disk applications from a scientific perspective, offering enhanced durability and reliability. However, NiCoCr alloy offers improved machinability and welding properties [**10**] while still providing good strength and resistance to high-temperature environments. Thus, the study could suggest that NiCoCr alloy might be a better investment in certain circumstances.

Based on the findings of this study, there are several potential directions for future research to further investigate the application of these results.

- **Mixed NiCoCr alloy-NiCrFe alloy Configuration**: It is worth considering the composition of the rotor assembly in such a way that not all parts are made from the same material. This could result in comparable performance at lower costs. Sensibly alternating parts made of NiCrFe alloy, such as those more subject to stresses like TW1 and TW3, with parts less affected by stresses, made of NiCoCr alloy, could reduce production costs for EthosEnergy in the manufacturing of gas turbine rotors.
- **3D Steady-State Analysis**: A 3D steady-state analysis could be performed on TW3, and secondarily on TW1, with a specific focus on creep and membrane stress. These are the most critical parts, and a 3D analysis would provide a more accurate structural evaluation and identify other potential critical areas.
- **Cost-Benefit Analysis**: Assessing the economic implications of switching from NiCrFe alloy to NiCoCr alloy, including manufacturing costs and potential performance benefits. This study focuses on the operational phase, but manufacturing, assembly, and maintenance costs could also be analyzed.

7 Bibliography

Paper [**1**] ,
author = "Marija Živic, Antun Galovic, Zdravko Virag",
title = "Detailed analysis of the effect of the turbine and compressor isentropic efficiency on the thermal and exergy efficiency of a Brayton cycle",
year = "2014",

Paper [**2**] ,
author = "Wesley R. Bussman, Charles E. Baukal Jr, John Zink",
title = "Ambient conditions impact CO and NOx emissions: part II",
month = jul,
year = "2009",

Paper [**3**] ,
author = "Douglas L. Straub, Karen A. Thole, James Black, Jason Town, Tom Shih",
title = "State-of-the-Art Cooling Technology for a Turbine Rotor Blade",
month = jun,
year = "2017",

Paper [**4**] ,
author = "Priyaranjan Sharma",
title = "Evaluation of WEDM performance characteristics of NiCoCr alloy for turbine disk application",
month = dec,
year = "2015",

Paper [**5**] ,
author = "Amr Elhefny, Guozhu Liang",
title = "Stress and deformation of rocket gas turbine disc under different loads using finite element modelling",
month = mar,
year = "2013",

Paper [**6**] ,
author = "Ali P. Gordon, Eric P. Williams, Michael Schulist",
title = "Applicability of Neuber's rule to thermomechanical fatigue",
month = jun,
year = "2008",

Paper [**7**] ,
author = "O. Belmonte, I. Remolar, J. Ribelles, M. Chover, M. Fernández ",
title = "Efficiently using connectivity information between triangles in a mesh for real-time rendering",
month = nov,
year = "2004",

Paper [**8**] ,
author = "M. K. Naidu, D. SanthaRao, J. KanthaRao",
title = "Stress Analysis of Gas Turbine Wheel",
year = "2013",

Paper [**9**] ,
author = "Mohammed Talal, Ziad Shakeeb Al Sarraf , Sabah M. Jamil",
title = "Finite Element Simulation and Stress Analysis of Gas Turbine Blade Due to Centrifugal Force",
month = jul,
year = "2023",

Paper [**10**] ,
author = "Z. Long, D. Fu, P. Ma, Z. Zhong ",
title = "Hot workability of IN706 alloy",
year = "1997".